Published in final edited form as:
J Phys Chem B. 2009 October 29; 113(43): 14421–14430. doi:10.1021/jp9050098.

A thermodynamic perspective on the dock-lock growth mechanism of amyloid fibrils

Edward P. O'Brien[1,2], **Yuko Okamoto**[3], **John. E. Straub**[4], **Bernard R. Brooks**[2], and **D. Thirumalai**[1,5,*]

[1]Biophysics Program, Institute for Physical Science and Technology, University of Maryland, College Park, MD 20742

[2]Laboratory of Computational Biology National Heart Lung and Blood Institute National Institutes of Health, Bethesda, MD 20892

[3]Department of Physics Nagoya University, Nagoya, Japan

[4]Department of Chemistry, Boston University, Boston, MA 02215

[5]Department of Chemistry and Biochemistry, University of Maryland, College Park, MD 20742

Abstract

The mechanism of addition of a soluble unstructured monomer to a preformed ordered amyloid fibril is a complex process. Based on the kinetics of monomer disassociation of Aβ(1 — 40) from the amyloid fibril, it has been suggested that deposition is a multi-step process involving a rapid reversible association of the unstructured monomer to the fibril surface (docking) followed by a slower conformational rearrangement leading to the incorporation onto the underlying fibril lattice (locking). By exploiting the vast time scale separation between the dock and lock processes and using molecular dynamics simulation of deposition of the disordered peptide fragment ^{35}MVGGVV^{40}, from the Aβ peptide, onto the fibril with known crystal structure we provide a thermodynamic basis for the dock-lock mechanism of fibril growth. Free energy profiles, computed using implicit solvent model and enhanced sampling methods, with the distance (δ_C) between the center of mass of the peptide and the fibril surface as the order parameter, show three distinct basins of attraction. When δ_C is large the monomer is compact and unstructured, and the favorable interactions with the fibril results in stretching of the peptide at $\delta_C \approx 13$ Å. As δ_C is further decreased the peptide docks onto the fibril surface with a structure that is determined by a balance between intrapeptide and peptide fibril interactions. At $\delta_C \approx 4$ Å, a value that is commensurate with the spacing between β-strands in the fibril, the monomer expands and locks onto the fibril. Using simulations with implicit solvent model and all atom molecular dynamics in explicit water, we show that the locked monomer, which interacts with the underlying fibril, undergoes substantial conformational fluctuations and is not stable. The cosolutes urea and TMAO destabilize the unbound phase and stabilize the docked phase. Interestingly, small crowding particles enhance the stability of the fibril-bound monomer only marginally. We predict that the experimentally-measurable critical monomer concentration, C_R, at which the soluble

*Corresponding author: Institute for Physical Science and Technology, University of Maryland, College Park, MD 20742, phone: 301-405-4803; fax: 301-314-9404; thirum@umd.edu.

unbound monomer is in equilibrium with the ordered fibril, increases sharply as temperature is increased under all solution conditions.

Proteins and peptides, that are unrelated by sequence or structure, form morphologically similar fibrillar structures upon aggregation [1–3]. The emergence of a global cross β-structure, that is the characteristic of all fibril forming proteins including those that are associated with distinct strains, suggests that their growth processes must be similar. Experiments on Aβ amyloid forming protein [4] have found that the process of monomer addition to an elongating amyloid fibril (Fig. 1) is kinetically complex involving distinct stages of growth with substantial structural transformations. More generally the cascade of events involving association of monomers into soluble oligomers and the formation of protofilaments and eventually fibrils results in a hierarchy of structures. Nevertheless, the overall association of a monomers with amyloid fibrils can be approximately described using two distinct timescales [5, 6]. Based on kinetic experiments involving $A\beta$-peptides, Lee and Maggio [5] envisioned that the growth of fibrils occurred by a sequential process involving two distinct steps that were pictorially described as the dock-lock growth mechanism. On a relatively fast timescale a monomer reversibly binds (or docks) to the fibril surface. A second slower timescale is associated with the lock process, which presumably involves structural rearrangements within the monomer leading to a greater binding affinity for the fibril [5–7]. Upon completion of the irreversible lock process the monomer adopts the β-strand conformation that is commensurate with the underlying fibril structure. The dock-lock growth process can be schematically shown as

$$A\beta^S \rightleftharpoons A\beta^D \rightarrow A\beta^F \quad (1)$$

where $A\beta^S$ and $A\beta^D$ represent the monomer in solution and in the docked phase respectively, and $A\beta^F$ is the structure adopted in the amyloid fibril.

The pictorial description in Eq. 1 is simplistic because it is likely that in both the major stages of deposition and growth there is a great deal of conformational fluctuations [6]. The plausibility for a dock-lock mechanism of fibril growth comes solely from bulk experiments, which show that the kinetics of monomer dissociation from a fibril can be fit by a sum of two or three exponentials [5, 6]. In addition, there is a paucity of data for the structural rearrangements that occur in the transition from the disordered soluble monomer to $A\beta^D$ or $A\beta^F$ [5, 6, 8]. Measuring such conformational changes is hampered by the inherently low concentration of fibril-bound monomer in the docked phase, and the length scale of the structural rearrangements involved in the dock-lock transition [5, 6].

Molecular simulations are ideally suited for providing structures, energies, and dynamics of the process of monomer addition to a fibril [9–19]. These studies have given considerable insights into the mechanisms of formation of amyloid fibrils. For example, in several previous computational studies we investigated many aspects of the early events of amyloid formation, including monomer addition to preformed structured oligomers [11], and the effect of urea on these species [9]. Results from these studies suggest that even oligomer growth can be described by a dock-lock mechanism. More recently, we have shown using

lattice models that fibril growth occurs globally by a dock-lock process with considerable structural heterogeneity in the rearrangement from the monomer to fibril [20].

Here, we use simulations to provide a thermodynamic basis for the global dock-lock mechanism of fibril growth. Although growth is an inherently kinetic process the clear separation in the time scales between the dock and lock process allows us to examine free energy and structural changes as the monomer interacts with the template fibril surface. The basic premise of our work is that the growth of fibrils occurs by addition of one monomer at a time. While more complex processes, including association between two protofilaments, can be envisioned current experiments [7] suggest that unstructured monomers add one at a time. With this assumption, we study the thermodynamics of the addition of a disordered Aβ monomer that is added to a preformed fibril surface. The availability of molecular structures [21] enables us to monitor the energetic and structural changes in the monomer as it attaches to the fibril. Using Multiplexed Hamiltonian Replica Exchange (MhREX) simulations [22, 23], we sample the reversible association/dissociation of a peptide (MVGGVV) from the Aβ protein to a fibril whose structure has recently been determined at atomic resolution [21]. The use of an implicit solvent model and enhanced sampling methods allows us to fully characterize the thermodynamics of the process under a variety of solution conditions.

Our simulations reveal a number of novel features of the thermodynamics of amyloid growth. The dock-lock mechanism is manifested as three basins in a free energy profile, which monitors the reversible work related to bringing a monomer to the fibril surface. The three basins correspond to two substate basins of the docked monomer and a locked phase in which the monomer adopts an extended anti-parallel conformation with modest β-strand content. As envisioned in the experimental study [5], there is a great deal of structural diversity in the reversible docking stage. The dock $\rightarrow$ lock transition is a disorder to order transition that involves an increase in the end-to-end distance of the monomer that is driven by the favorable peptide-fibril interactions. The free energy barrier separating the docked and locked phases arises largely from the loss of favorable intra-peptide interactions of the monomer that is deposited onto the surface.

To further shed light on the energetics governing monomer addition we have probed the influence of cosolvents (urea and Trimethylamine N-oxide (TMAO)) and molecular crowders on the free energy profiles. Surprisingly, a modest concentration (0.75 M) of either urea or TMAO stabilizes the locked phase, while molecular crowding only marginally stabilizes the docked phase. The thermodynamics of amyloid formation can be inferred by measuring the equilibrium between the amyloid fibril and the soluble monomer as shown by Wetzel and coworkers [24]. A measure of the free energy of stability of the fibril structure is the critical monomer concentration, C_R, which is the concentration of soluble monomer that is in equilibrium with the amyloid fibril [24]. We show that C_R is strongly temperature dependent, and exhibits weak cosolvent dependence. Our study provides a conceptual framework for interpreting the thermodynamics of fibril formation.

Computational Methods

Fibril model

To illustrate the structural transformations in a monomer interacting with a fibril, we chose a six residue peptide (^{35}MVGGVV^{40}) fragment from the Aβ[4] protein that forms amyloid-like fibrils *in vitro*, and whose fibrillar structure is known to 2Å resolution [21]. We select a cross-section of this fibril's crystal structure (PDB code 2OKZ), two-by-three unit cells wide, made up of a total of twelve peptides, that lies perpendicular to the long fibril axis (Fig. 1). This leads to an approximately rectangular surface that is ~48 Å long by ~45 Å wide, and has the peptide backbones fully exposed to solvent.

The unit cell of the amyloid fibril crystal is monoclinic with angles α, β, γ of 90°, 96.9°, and 90°, respectively [21]. The unit cell distances a, b, c are 15.148, 9.58, and 23.732 Å, respectively [21]. We carry out simulations on a fibril surface that uses monoclinic periodic boundary conditions with the same α, β, γ angles as in the crystal and a, b, c values of 45.444, 125.0, 47.464 Å. This results in a fibril surface that has no lateral edges because it is infinite in the *xz*-plane (Fig. 1). Consequently, our simulations only probe monomer association to the surface of the fibril that is perpendicular to the long fibril axis. This is justified based on the experimental observations that, under certain conditions, soluble monomers deposit largely on the backbone exposed surface of the fibril. The probability of lateral association of protofilaments is likely to be small during the late stages of fibril elongation [25, 26].

Implicit Solvent Model

The CHARMM 22 force-field [27] in conjunction with grid based correction maps (CMAP) to the backbone dihedral angles [28], that reproduce *ab initio* computed Ramachandran plots of dipeptides, is used to model bonded and non-bonded protein interactions. It is difficult to carry out all-atom explicit solvent simulations that adequately sample the equilibrium conformational space. Hence, we use an all-atom representation of the protein and include the effects of solvent using a Generalized Born implicit solvent model (GBSW) [29]. With this simplification the simulation times can be greatly extended allowing us to obtain converged results for various thermodynamic quantities.

Mimics of cosolvents Urea and TMAO for use in implicit solvent simulations

For use in implicit solvent simulations we introduce a novel way to model interactions involving cosolvents and proteins. We model urea and TMAO as spherical particles that interact with atoms in the peptide via

$$V(r_{ij}) = 4\varepsilon_{ij}\left[\left(\frac{\sigma_{ij}}{r_{ij}}\right)^{12} - \lambda\left(\frac{\sigma_{ij}}{r_{ij}}\right)^{6}\right], \quad (2)$$

where r_{ij} is the distance (in Å) between a protein atom *i* and a cosolute molecule *j*, ε_{ij} is the interaction strength between them, $\lambda = 1$, and the values of σ_{ij} are computed using the Lorentz-Brethlot mixing rules [30]. Interactions between the osmolyte molecules are

repulsive (i.e. δ=0 and ε_{ij} =0.1). The size of urea and TMAO is σ_i =7 Å. The larger collision diameter, compared to molecular volume and partial molar volume estimates of TMAO and urea molecules [31], approximately accounts for the ordered first solvation shell of water surrounding the cosolutes.

The ε_{ij} values in Eq. 2 are chosen so that $\delta g_{tr,E}(0M \rightarrow 1M) \approx \delta g_{tr,C}(0M \rightarrow 1M)$, where $\delta g_{tr,C}(0M \rightarrow 1M)$ is the computed free energy of transferring the individual protein groups (backbone or side chain) from pure water to aqueous osmolyte solution at 1 M, and $\delta g_{tr,E}(0M \rightarrow 1M)$ is the experimentally measured value [32, 33]. We calculated $\delta g_{tr,C}$ using the Widom particle insertion technique [34], where $\delta g_{tr,C} = -k_B T \ln \int ds_{N+1} exp(-\Delta U/(k_B T))_N$, with ΔU being the non-bonded interaction energy (i.e. the Lennard-Jones energy) between a system containing N TMAO (or urea) molecules and a randomly inserted protein group. The quantity $exp(-\Delta U/(k_B T))$ is averaged over all system configurations of the cosolutes. Because we are using an implicit solvent model and solutions at fairly low osmolyte concentrations (0.75 M) we are able to obtain converged $\delta g_{tr,C}$ data [35]. Typically, 10^5 insertion attempts were necessary to obtain $\delta g_{tr,C}$ values that had a standard error of less than 10^{-5} *kcal/mol* [34]. Thus, many ε_{ij} parameters were tested until $\delta g_{tr,C}$ was within 0.5 cal/mol of $\delta g_{tr,E}$. The ε_{ij} parameters are listed in Table I.

This approach, while accounting for the particulate nature of cosolvents and the free energy of interaction between cosolvents and proteins, does not include molecular details of the cosolvent that control some of the fine details of the liquid structure (as measured by radial distribution functions) around the protein. For example, orientation-dependent interactions such as hydrogen bonding between cosolvent-peptide and cosolvent-water are neglected. Our method is an implicit solvent representation of cosolvents. These approximations can change the fine details of the free energy landscape, especially on the length scale of a water molecule. However, we expect gross features, such as the conformational fluctuations in the monomer in the various phases and the behavior with changing solution conditions to be captured.

Simulation Details

To enhance sampling efficiency low friction Langevin simulations [36], with a damping constant of 1.2 ps^{-1}, were carried out in conjunction with Multiplexed Hamiltonian Replica Exchange (MhREX) [22, 23]. In an MhREX run, multiple independent trajectories (replicas) are simulated at different temperatures and with different Hamiltonians [22]. Periodically, the coordinates between the replicas are swapped according to a set of rules that preserve detailed balance [22].

We used three temperature windows (280, 325, and 380 K) and twelve different Hamiltonians (denoted $H_{i=1,..,12}$). For each temperature-Hamiltonian pair two independent trajectories are generated simultaneously. Thus, a total of 72 replicas are simulated in one MhREX run. The Hamiltonians differ only in the potential energy term $E_{U,i}=0.5K_{U,i}(\delta_C-\delta_C^i)^2$, that restrains the center-of-mass of the monomer, defined using the C_α atoms of the monomer backbone, to a distance δ_C^i (in Å) along the *y*-axis from the fibril surface (Fig. 1). $K_{U,i}$ is the force constant (in *kcal*/Å) in the i^{th} Hamiltonian. The (δ_C^i, $K_{U,i}$)

pairs for i =1,.., 12 are (1.75,3.00), (3.00,3.50), (4.50,2.50), (6.00,2.5), (7.50,3.5), (9.00,3.25), (10.0,2.75), (11.0,1.5), (13.5,1.2), (15.0,1.0),(17.0,1.0),(19.0,1.0), respectively. We alternate the swaps between temperatures and Hamiltonians. Random shuffling between replicas at the same temperature and Hamiltonian are carried out at each swapping attempt. Every 143 integration time-steps swapping of system coordinates between temperatures or between Hamiltonians is attempted. In all, 55,000 swaps are attempted, with the first 5,000 discarded to allow for equilibration. The swapping acceptance ratio's were between 10% and 40%. Trajectories are simulated in the canonical (NVT) ensemble, and the equations of motion are integrated with a 2 fs time-step. The total simulation time per replica is 14.3 ns and the sum total simulation time (over all replicas) is 1.03 μs. We use the CHARMM software package (version c33b2) to generate the trajectories [30]. An in-house perl script was written to run MhREX.

Explicit solvent simulations

All-atom explicit solvent simulations were carried out in the NVT ensemble at 300 K using the CHARMM program in conjunction with the CHARMM 22 force field. Cubic periodic boundaries were used in these simulations with box dimensions of approximately 54 × 28 × 28 Å. Non-bonded interactions were truncated at 12 Å with a switching function applied starting at 10 Å. The TIP3P water molecule was used to model water and the SHAKE algorithm was used to hold covalent bonds involving hydrogen fixed at their equilibrium length. A 2 fs integration time-step was used during dynamics and each trajectory was 30 to 45 ns in length. The same peptide and crystal structure were used as in the implicit solvent model simulations except that only three β-sheets from the fibril were used. Thus, there are a total of six peptides in the simulation box. Five of the peptides were fixed during the simulation and thus exhibited no structural fluctuations. The fourth monomer was unrestrained during the simulations. Four independent trajectories were produced starting from two different initial configurations of the system. In one configuration the simulation was started from the monomer fully locked into the fibril, having the coordinates of the crystal structure. In the other configuration the monomer was displaced 4 Å from the fibril surface along the long fibril axis. Two trajectories were started from these two initial configurations using different random velocity assignments, resulting in four independent simulations.

Potential-of-mean-force (PMF) and Structural probes

Thermodynamic properties of the system are computed using the WHAM equations [37, 38]. The PMF is computed as $F(\delta_C) = -k_B T \ln[P(\delta_C)]$, where $P(\delta_C)$ is the probability of finding the monomer at a distance δ_C from the fibril surface. We used STRIDE to compute the secondary structure content of the monomer [39]. To examine the global orientation of the monomer, relative to the fibril surface, we compute the two-dimensional free energy surface ($F(\delta_C, cos(\theta)) = -k_B T \ln[Z(\delta_C, cos(\theta))/Z(\delta_C)]$ as a function of δ_C and θ, the angle formed between a vector normal to the fibril surface and a vector connecting the C_α atoms of the *N*-terminus and *C*-terminus (Fig. 1). Backbone contacts between the added monomer and the peptides on the surface of the fibril are assumed to be formed if the C_α atoms between peptides are within a distance of 6 Å. Numbering each residue in a peptide from 1 to 6, starting from the N-termini, in-register parallel backbone contacts occur if residue i, the

residue number, of strand *j* is in contact with residue *k* of strand *l* and *i* = *k*. Similarly, in-register anti-parallel contacts occur between strands *j* and *l* if *i* and *k* are in contact and *k* =7 − *i*.

Results and Discussion

The Potential of Mean Force (PMF) of monomer addition to the fibril surface has multiple basins of attraction

The PMF, $F(\delta_C)$, that gives the reversible work required to bring the monomer to a distance δ_C above the fibril surface (Fig. 1), shows multiple basins of attraction as T is changed from 280 K to 380 K (Fig. 2). There are three distinct basins at temperatures below 340 K (Figs. 2A and 2B). The minimum in the first basin (B_1 in Fig. 2A) is at δ_C = 7.1 Å, and the other two basins (B_2 and B_3) are at 5.5 and 3.9 Å, respectively. At 280 K the free energy barrier separating B_1 and B_2 is ~1.2 kcal/mol. At higher temperatures the barriers decrease, and at 380 K there is virtually no free energy barrier separating the basins. When δ_C < 3.9 Å the PMF increases due to the unfavorable steric interactions between the monomer and the fibril surface. The PMF also increases sharply at δ_C > 9 Å, where there are very few contacts between the monomer and the fibril.

In order to associate the features in the PMF with the dock-lock picture it is necessary to examine the structural transitions that occur as δ_C changes. If the basins observed in the $F(\delta_C)$ profile correspond to the docked and locked phases, we expect structural changes in the monomer when δ_C decreases from 7.1 Å to 3.9 Å. The fibril-bound monomer undergoes a global expansion, with an increase in R_g from 4.6 Å → 5.7 Å, as it goes from B_1 to B_3 (Fig. 3). The end-to-end distance also dramatically increases from 8 Å to 13 Å (Fig. 3B). It is significant that the maxima in the derivatives of $\frac{dR_g}{d\delta_C}$ and $\frac{dR_{ee}}{d\delta_C}$, in the range of 9 > δ_C > 3.9 Å, occur at δ_C = 6.2 and 4.7 Å (computed using Fig. 3, data not shown). The positions of these maxima coincide with the locations of the free energy barriers in the PMF (Fig. 2A), which suggests that the barriers form during the process of expansion of the monomer as it interacts with the fibril surface.

We examine the free energy profile of R_{ee} at fixed δ_C values ($F(R_{ee}|\delta_C)$) in Figs. 2C, 2D, and 2E. These figures show that additional basins are present in the free energy surface that are not evident when projected onto the one-dimensional order parameter δ_C. For example, at δ_C = 3.7 Å and δ_C 5.5 Å (basins B_1 and B_2) $F(R_{ee}|\delta_C)$ exhibits two or more basins. Thus, there are numerous metastable states in the dock-lock process. Based on the global structural changes in R_g and R_{ee}, we tentatively designate the monomer as unbound if δ_C > 9 Å, docked if the monomer is in the range of 9 > δ_C > 5 Å, and locked when δ_C < 5 Å.

Free energy landscape during the growth process

Surprisingly, an additional structural transformation in the monomer, that is not evident in $F(\delta_C)$, is revealed by the $R_g(\delta_C)$ and $R_{ee}(\delta_C)$ profiles. In the range of 16 > δ_C > 9 Å the monomer is 'stretched', with R_g and R_{ee} values close to that found in an extended β-strand (Fig. 3). Examination of the backbone-backbone contacts that occur between individuals residues of the monomer and the fibril (Fig. 4) shows that the N-terminal methionine residue

contacts the fibril surface when δ_C is between 12 and 14 Å. The favorable interaction of the N-terminal residue with the fibril surface leads to the chain expansion observed in $R_g(\delta_C)$ and $R_{ee}(\delta_C)$ when $\delta_C \sim 12$ Å (Fig. 3).

To examine the global orientation of the monomer as it interacts with the fibril surface we show, in Fig. 4B, the free energy surface ($F(\delta_C, cos(\theta))$) as a function of δ_C and $cos(\theta)$, where θ is the angle formed between a vector normal to the fibril surface and the *N* to *C*-termini vector of the monomer (see Fig. 1). When $cos(\theta) = -1$ (1) the monomer is oriented towards (away from) the surface (see Fig. 1). A value of $cos(\theta) = 0$ implies that the monomer is parallel to the fibril surface. At the farthest distances from the fibril ($\delta_C > 19$ Å), the orientation of the monomer is randomly distributed (Fig. 4B) as indicated by the lack of a dominant free energy basin in $F(\delta_C, cos(\theta))$. However, at $\delta \approx 12$ Å and $cos(\theta) = 1$ there is a basin, indicating that the monomer's *N* to *C*-termini vector is pointing away from the fibril surface (Fig. 4B). Thus, the *N*-terminus is closest to the fibril surface in the 'stretched' state. As δ_C decreases to 4 Å, basins with values of $cos(\theta) \approx 0$ are favored, which shows that the monomer is aligned parallel to the fibril surface.

Monomer deposition to the fibril surface results in multiple structural transitions

We characterize the structural changes that the monomer undergoes while interacting with the fibril using the number of peptide-fibril contacts, and the number of in-register peptide-fibril backbone contacts. In the range of $16 > \delta_C > 9$ Å, the monomer makes very few contacts with the fibril surface (data not shown). Several non-specific peptide-fibril contacts are made that are energetically favorable (Fig. 5B). Because δ_C is large (relative to R_g) the peptide must extend to make contact with the fibril, as evidenced by the increase in R_g and R_{ee} (Fig. 3). In the extended conformations there is a significant decrease in the favorable intra-peptide interactions (Fig. 5B). Upon reducing δ_C in the range of $9 > \delta_C > 6.2$ Å, the monomer docks onto the fibril surface (Fig. 2). In the process, the monomer undergoes a dramatic reduction in R_g from a maximum of 5.7 Å, when $\delta_C > 9$ Å, to 4.6 Å (Fig. 3). The reduction in R_g is accompanied by an increase in favorable enthalpic interactions both within the monomer and between the monomer and the fibril (Fig. 5). When hopping between basins B_1 and B_2 in the docked phase, the monomer undergoes only small structural rearrangements, as measured by $R_g(\delta_C)$ and $R_{ee}(\delta_C)$ (Fig. 3). There are fewer in-register backbone contacts in the docked phase as compared to the locked phase (Figs. 4A and 4B).

The monomer undergoes a large scale structural rearrangement as it locks onto to the fibril surface ($5.0 > \delta_C > 3.0$ Å). In addition to an increase in R_g (Fig. 3), favorable intra-peptide interactions are lost (Fig. 5B), and are replaced by peptide-fibril contacts and interactions (Figs. 4A and 5B). The monomer forms antiparallel in-register backbone contacts (Fig. 4A) in agreement with the monomer orientation in the crystal structure [21]. In Fig. 2 we show monomer-fibril configurations corresponding to the unbound, docked and locked phases. Note that the 'stretched' conformation shown in Fig. 2 correlates with the expanded R_g in Fig. 3.

To analyze the stability of the docked monomer, we analyze the secondary structural content as a function of δ_C using the STRIDE program [39]. For $\delta_C > 9$ Å the monomer is unstructured and is dominated by random coil (> 60%) with moderate turn content (< 40%).

In the docked phase, turn content dominates (≈60%) and the coil content drops to ≈35%. In the locked phase the peptide is predominantly a random coil (≈80%), turn content is around 10%, and β-bridge content around 10%. Although the locked monomer does form an antiparallel β-sheet with the fibril, with frayed ends, the structure is not stable in the simulations. Thus, in contrast to the structure of a peptide in the fibril crystal structure the β-strand content in the simulated monomer is small even after locking is complete. There are three possible reasons for the instability of the β-strand in the locked phase in our simulations. First, in experiments the width of fibrils is finite consisting of just a few β-sheets whereas in our simulations the fibril surface is essentially infinite. As a result, in our simulations a single monomer can bind to multiple sites on the surface leading to an increase in the binding entropy that can compensate for the energy gain that arises from forming an in-register β-sheet with another monomer in the fibril. Thus, the free energy of the added monomer can be minimized by making multiple out-of-register backbone contacts with different strands in the fibril-leading to small β-strand content. Secondly, the absence of additional monomers, which could offer a self-crowding environment for the docking monomer, enhances the conformational fluctuations thus decreasing the β-strand content. Self-crowding would enhance the stability of the monomer once it forms a structure that is commensurate with the underlying fibril lattice.

Besides the two physical reasons, it is likely that the GBSW implicit solvent model is inaccurate to describe the stability of the fibril. To test whether the observed instability is due to the use of the implicit solvent model we performed all-atom explicit solvent molecular dynamics simulations of the monomer on a fibril of finite width, shown in Fig. 6, at 300 K. We generated four independent trajectories each 45 ns in simulation time. Two of the trajectories were started with the monomer in the locked phase (i.e. in the crystal conformation) and two were started with the center of mass of the monomer displaced by 4 Å along the fibril axis away from the fibril surface. During the simulations, the two displaced monomers come into contact with the fibril surface. However, on the simulation time scale they did not acquire β-strand content or interstrand hydrogen bonds (data not shown). Of the two trajectories that are started in the locked phase, one exhibits a decrease in β-strand content while the other stays fully locked. While these explicit solvent simulations are by no means ergodic, these results suggest that perhaps even in explicit solvent simulations the monomer is not stable as a β-strand on the fibril surface. These preliminary findings show that it is difficult to accurately describe the stability of fibrils using current force fields.

The overall goal of this study is to provide a picture of the structural changes that occur as the monomer starts to interact with the fibril lattice and not to obtain accurate estimate of the stability of the locked phase. The various structural probes used here give a view of the changes in the free energy profile as δ_C decreases. Furthermore, we show below the critical concentration calculated from these simulations exhibit realistic changes with solution conditions, which suggests that the present simulations capture qualitatively the complexity of the dock-lock mechanism.

The free energy barrier separating the docked from locked phases is largely enthalpic

To determine the origin of the free energy barriers separating the docked and locked phases (Fig. 2) we compute the potential energy (E_P) and entropic (TS) contributions to F (δ_C). The profiles of E_P (δ_C) and TS(δ_C) (Fig. 5A) have maxima at the same locations as the basins in F (δ_C) (Fig. 2). At $\delta_C \approx 6$ Å, the maximum in E_P is greater than in TS, indicating that potential energy gives rise to the free energy barriers separating the docked and locked phases in F (δ_C). Interestingly, the monomer gains entropy upon reaching the top of the barrier from the docked phase in F (δ_C) (Fig. 5A). However, the monomer loses entropy upon locking onto the fibril surface as indicated by $T\,\Delta S_{D\to L} \equiv T\,(S_L - S_D)$, where $S_i = \sum_{\delta_{i,l}}^{\delta_{i,u}} S(\delta_i) e^{-\beta F(\delta_i)}$ and $\delta_{i,u}$ and $\delta_{i,l}$ correspond to the upper (u) and lower (l) bounds in δ_C that separate the docked and locked basins in the F (δ_C) profile. At 300 K, $T\,\Delta S_{D\to L}$ = −2.6 kcal/mol, and at 380 K $T\,\Delta S_{D\to L}$ =−6.7 kcal/mol.

To determine the molecular origin of the barriers in F (δ_C) we deconvolute the E_P (δ_C) profile into contributions from the monomer internal energy (E_M (δ_C)), that is the interaction energy of the monomer with itself, and the monomer-fibril interaction energy (E_{MF} (δ_C)). These profiles (Fig. 5B) clearly show that the docked phase is energetically stabilized by internal monomer interactions and monomer-fibril interactions, while in the locked phase favorable internal monomer interactions are lost and replaced by monomer-fibril interactions. Consequently, it is the interplay of these two energies as the monomer undergoes conformational changes that contributes to the potential energy barrier separating the docked and locked phases.

Urea and TMAO stabilize the fibril-bound monomer

The cellular environment, besides containing large biomolecules, also contains osmolytes that can dramatically effect protein function [40], stability [40, 41], and amyloid formation [42–44]. Naturally occurring osmolytes, such as TMAO and urea, can be found in a variety of organisms at concentrations from 0 to 6 M [40, 45]. Therefore, to carry out simulations at physiologically relevant concentrations, we simulate the process of monomer addition in aqueous urea and TMAO solution at 0.75 M using a coarse grained model for urea and TMAO(Eq. 2).

Urea and TMAO increase the stability of the locked phase relative to bulk (Fig. 7). In contrast, the unbound and docked states are destabilized in the presence of these osmolytes. Our simulations show that urea stabilizes the locked phase to a lesser extent than TMAO. This is due to the stronger interaction of urea (see Methods section) with the peptide and the fibril. For example, R_g of the unbound monomer is slightly greater in urea than in TMAO (data not shown), due to the stronger attraction between the urea molecules and the peptide. The greater affinity is reflected in the radial distribution function (RDF) between the cosolutes and the peptide groups (O=C-N-H) of the protein backbone. The first peak in the RDF, located at r = 7.5 Å, indicates that urea preferentially interacts with the backbone and binds more strongly than TMAO (data not shown).

The observation that urea stabilizes the locked species requires an explanation because typically denaturants destabilize the fold state of globular proteins. The tendency of urea to denature globular proteins can be understood in terms of its enhanced preference for the protein backbone and solvation of hydrophilic residues compared to water [46, 47]. Thus, urea effectively decreases favorable intrapeptide interactions, and consequently at high enough concentration results in unfolding of the protein. In contrast to the urea-protein interaction, the stability of the docked phase is determined by at least four free energy scales; they are the intrapeptide, monomer-solvent, monomer-fibril, and fibril-solvent interaction energies. The stability of the docked phase depends on how these free energy scales vary as a function of cosolvents, such as urea and TMAO, and their concentration. Our results suggest that small amounts of urea and TMAO tend to favor monomer-fibril interactions to a greater extent than others. We expect that at high concentrations of osmolyte the unbound species may be stabilized which would result in the instability of the monomer bound to the fibril. Indeed, there is experimental evidence for such a non-monotonic dependence on the osmolyte concentration [43].

To contrast the effect of specific interactions between urea and TMAO on the stability of the docked and locked states we also carried out simulations to probe the influence of small crowding particles on their stabilities. The interaction between the crowding particle and the peptide atom is mimicked using Eq. 2 with $\varepsilon_{ij} = \varepsilon = 0.1$ kcal/mol and $\lambda = 0$. At a crowder volume fraction of $\phi_C = 0.14$ (concentration of 0.75 M), the PMF indicates that inert-crowding particles only marginally stabilize the docked phase, with respect to bulk, and destabilize the locked phase.

The effect of TMAO and urea on the critical concentration C_R

When amyloid fibrils reach equilibrium (when the rate of monomer addition to the fibril equals the rate of dissociation) some number of monomers remain unbound in solution. The equilibrium concentration of the soluble unbound monomers is the critical concentration, C_R. One can relate C_R to the equilibrium constant of dissociation of a monomer from the fibril [24]. Wetzel and coworkers have used this observation to map the regions in $A\beta_{1–40}$ that harbor amyloidogenic tendencies [8, 24]. The free energy profiles computed in our simulations allow us to calculate the relative changes in C_R as the cosolvent concentration or temperature is varied. From the density of monomer a distance δ_C from the fibril surface, C_R can be calculated using

$$C_R = C\int_{\delta_M}^{\delta_U} e^{-\beta F(\delta_C)} d\delta_C, \quad (3)$$

where C is the bulk density of peptide in solution, $\beta = 1/k_BT$, where k_B is Boltzmann's constant, T is the temperature of solution condition, and $F(\delta_C)$ is the PMF. Based on our previous results using multiple structural probes we set δ_M, the boundary between the docked and unbound species, to 9 Å. We set δ_U to 22 Å since this is the largest δ_C value appreciably populated in our MhREX simulations due to the harmonic restraint with a minimum at $\delta_C^i = 19$ Å. The value of δ_U defines the volume accessible to the peptides during the simulation and is thus directly related to the bulk density C. To test the robustness of the

results presented below a variety of δ_M and δ_U were tested (data not shown). The trends in computed R were unaffected by moderate changes (± 5 Å) in δ_M and δ_U.

The relative change in C_R, upon a change in solution conditions (altering cosolute concentration of temperature) can be computed without determining C in Eq. 8, using

$$R=\frac{C_{R,j}}{C_{R,i}}=\frac{\int_{\delta_M}^{\delta_U} e^{-\beta_j F_j(\delta_C)} d\delta_C}{\int_{\delta_M}^{\delta_U} e^{-\beta_i F_i(\delta_C)} d\delta_C}, \quad (4)$$

where $C_{R,j}$ ($C_{R,i}$) is the value of C_R in solution condition j (i) and F_j (F_i) is the corresponding free energy profile.

In Figs. 8A and B the ratio of the critical concentration relative to either C_R in bulk or C_R at 300 K is shown as a function of temperature for the various solution conditions. Holding the solution temperature fixed below approximately 340 K we find that upon addition of cosolutes to solution $R_1(= C_R(T\,|cosolute)/C_R(T\,|Bulk))$ decreases (Fig. 8A). For example, at 300 K R_1 equals 0.3, 0.5, and 0.2 for crowder, TMAO and urea respectively. Thus, addition of the cosolutes at these temperatures decreases C_R, which is in accord with the stabilization observed of the fibril-bound monomer. However, at higher temperatures R_1 is greater than 1, which means at these temperatures addition of these cosolutes increases the critical concentration.

Holding cosolute concentration constant we find that upon an increase in temperature $R_2(= C_R(T)/C_R(T = 300K))$ is monotonically increasing (Fig. 8B). For example, changing T from 300 K to 380 K leads to R_2 values of 38.5, 160, 638 and 526 in bulk, crowder, TMAO and urea solutions respectively. Thus, increasing temperature increases C_R under all solution conditions. Interestingly, the locked phase can still be stabilized despite the increase in C_R. For example, in bulk solution we find that increasing the temperature from 300 to 380 K results in a stabilization of the unbound and locked phases by 0.4 and 0.6 kcal/mol respectively. The docked phase on the other hand is destabilized by ≈ 0.9 kcal/mol. This result is important because it illustrates that C_R only measures the equilibrium constant of monomer association and cannot measure the equilibrium constants of the monomer in the docked and locked phases. Thus, increases in C_R do not always indicate destabilization of the locked phase. These predictions are amenable to experimental tests.

Conclusions

By exploiting the large separation in the time scales of the two major events (dock and lock) in the growth of amyloid fibrils, we have provided a thermodynamic description of monomer addition to a fully formed fibril. Although the results have been obtained by examining the addition ^{35}MVGGVV^{40} to a template fibril, the framework is expected to be of general validity. Because the structure of the unbound monomer is usually not commensurate with the fibril it follows that the monomer must undergo a cascade of structural transitions. Our simulations show that, surprisingly, even a small peptide can adopt a diverse set of conformations prior to locking onto the fibril. Because there is a great

deal of structural diversity in the docked and locked states it follows that the subsequent lock process must be dynamically heterogeneous. The diversity in the locking state, and hence in the growth of amyloid fibrils, could be assessed using single molecule experiments. In analogy with single molecule FRET experiments carried out on globular proteins, the monomer labelled with donor and acceptor dyes, with the fibril unlabelled, could be used to probe structural substates associated with the dock-lock process based on the distribution of FRET efficiencies and the dynamic transitions between them.

From the perspective of simulations, we have provided a novel method for computing interactions between cosolvents for use in implicit solvent simulations. Using this methodology, we showed that small concentrations of urea and TMAO, that are known to have opposing effects on protein stability, increase the stability of the locked phase. The use of implicit cosolute models and the free energy profiles may be particularly useful in the computation of C_R, the critical monomer concentration that is in equilibrium with the fibril. In a series of papers, Wetzel and coworkers exploited the thermodynamic equilibrium between A^S and A^F (reflected in C_R) for two Aβ(1-40) sequences that differ at a single position to probe the regions that are strongly amyloidogenic [24]. The same idea can be exploited to compare the effects of two solution conditions on the stability of fibrils. We have shown that the C_R values can be used to predict qualitatively the relative (with respect to a reference condition) stability of the fibril bound monomer under varying solution conditions. We predict that C_R is strongly temperature dependent. Thus, measurements of C_R as a function of temperature should be useful in predicting the energetics of fibril formation. The sensitivity of C_R to temperature and mutations can be used to map regions of proteins or peptides that harbor amyloidogenic tendency.

Although our simulations provide thermodynamic perspectives on the amyloid growth they are not without limitations. For example, using both atomistic and implicit solvation models we find that the β-strand content of the locked monomer does not reach the value found in the fibrils. There are two possible reasons for this discrepancy. (1) The current force fields are not accurate enough to describe stable fibrils. In order to ascertain that this is indeed the case we performed additional simulations, using implicit and explicit solvent models, to examine the stability of the monomer that is locked onto finite-sized fibrils. These simulations complement those that were done using the setup in Fig. 1. From multiple trajectories, with the implicit solvent model, we find that the locked monomer undocks after a finite time indicating that the system is kinetically unstable. We performed similar simulations using explicit solvent. Among the four independent trajectories, each 45*ns* in length, two were started with the center of mass of the monomer displace by about 4 Å away from the fibril along the fibril axis. The initial condition for the other two corresponded to an ordered locked structure. It was found that even when the initial condition corresponds to the monomer being locked the β-strand content decreased over time. Taken together these simulations suggest that the stability of the locked phase cannot be described using the force-fields that are used in simulations. (2) The peptide used here is predominantly hydrophobic, which implies that the stability of the fibrils arises largely from the non-specific dispersion interactions between the side chains. In a recent study, we showed that fibrils formed from largely hydrophobic peptides are not as stable as those from sequences

in which the inter peptide interactions involve hydrogen bonds. In particular, the heptamer from Sup35 which forms parallel β-strands are stabilized by a network of hydrogen bonds that result in the formation of a highly stable fibril. It is likely that a combination of both these factors lead to the kinetic instability of the fibril formed from $^{35}MV\,GGV\,V^{40}$ peptide. Nevertheless, the free energy landscapes derived here provide the plausible structural transitions that take place during the amyloid growth process and furnishes a thermodynamic perspective on the dock-lock mechanism.

Acknowledgments

We are grateful to Govardhan Reddy for useful discussions. This study utilized the high-performance computational capabilities of the Biowulf Linux cluster at the National Institutes of Health, Bethesda, Md. (http://biowulf.nih.gov). This work was supported in part by grants from the NIH to J.E.S. and D.T. (RO1GM076688-05), a NIH GPP Biophysics Fellowship and a NSF-East Asia and Pacific Summer Institutes Fellowship to E.O., and by the Intramural Research Program of the NIH, NHLBI.

References

1. Tycko R. Progress towards a molecular-level structural understanding of amyloid fibrils. Curr Opin Struc Biol. 2004; 14(14):96–103.
2. Chiti F, Dobson CM. Protein misfolding, functional amyloid, and human disease. Ann Rev Biochem. 2006; 75:333–336. [PubMed: 16756495]
3. Thirumalai D, Klimov DK, Dima RI. Emerging ideas on the molecular basis of protein and peptide aggregation. Curr Opin Struc Biol. 2003; 13(2):2003.
4. Citron M, Oltersdorf T, Haass C, McConlogue L, Hung AY, Seubert P, Vigopelfrey C, Lieberburg I, Selkoe DJ. Mutation of the beta-amyloid precursor protein in familial alzheimers-disease increases beta-protein production. Nature. 1992; 360:672–674. [PubMed: 1465129]
5. Esler WP, Stimson ER, Jennings JM, Vinters HV, Ghilardi JR, Lee JP, Mantyh PW, Maggio JE. Alzheimer's disease amyloid propagation by a template-dependent dock-lock mechanism. Biochem. 2000; 39(21):6288–6295. [PubMed: 10828941]
6. Cannon MJ, Williams AD, Wetzel R, Myszka DG. Kinetic analysis of beta-amyloid fibril elongation. Anal Biochem. 2004; 328(1):67–75. [PubMed: 15081909]
7. Collins SR, Douglass A, Vale RD, Weissman JS. Mechanism of prion propagation: Amyloid growth occurs by monomer addition. PLOS Biology. 2004; 2(10):1582–1590.
8. Wetzel R. Kinetics and thermodynamics of amyloid fibril assembly. Acc Chem Res. 2006; 39:671–679. [PubMed: 16981684]
9. Klimov DK, Straub JE, Thirumalai D. Aqueous urea solution destabilizes a beta(16-22) oligomers. Proc Natl Acad Sci USA. 2004; 101(41):14760–14765. [PubMed: 15465917]
10. Tarus B, Straub JE, Thirumalai D. Probing the initial stage of aggregation of the a beta(1035)-protein: Assessing the propensity for peptide dimerization. J Mol Biol. 2005; 345(5):1141–1156. [PubMed: 15644211]
11. Nguyen PH, Li MS, Stock G, Straub JE, Thirumalai D. Monomer adds to preformed structured oligomers of a beta-peptides by a two-stage dock-lock mechanism. Proc Natl Acad Sci USA. 2007; 104(1):111–116. [PubMed: 17190811]
12. Klimov DK, Thirumalai D. Dissecting the assembly of a beta(16-22) amyloid peptides into antiparallel beta sheets. Structure. 2003; 11(3):295–307. [PubMed: 12623017]
13. Bellesia G, Shea JE. Self-assembly of beta-sheet forming peptides into chiral fibrillar aggregates. J Chem Phys. 2007; 126(24)
14. Massi F, Klimov D, Thirumalai D, Straub JE. Charge states rather than propensity for beta-structure determine enhanced fibrillogenesis in wild-type alzheimer's beta-amyloid peptide compared to E22Q dutch mutant. Prot Sci. 2002; 11(7):1639–1647.

15. Baumketner A, Krone MB, Shea JE. Role of the familial dutch mutation E22Q in the folding and aggregation of the 15-28 fragment of the alzheimer amyloid-beta protein. Proc Natl Acad Sci USA. 2008; 105(16):6027–6032. [PubMed: 18408165]
16. Nguyen HD, Hall CK. Molecular dynamics simulations of spontaneous fibril formation by random-coil peptides. Proc Natl Acad Sci USA. 2004; 101(46):16180–16185. [PubMed: 15534217]
17. Fawzi NL, Yap EH, Okabe Y, Kohlstedt KL, Brown SP, Head-Gordon T. Contrasting disease and nondisease protein aggregation by molecular simulation. Acc Chem Res. 2008; 41(8):1037– 1047. [PubMed: 18646868]
18. Fawzi NL, Okabe Y, Yap EH, Head-Gordon T. Determining the critical nucleus and mechanism of fibril elongation of the alzheimer's a beta(1-40) peptide. J Mol Biol. 2007; 365(2):535– 550. [PubMed: 17070840]
19. Auer S, Dobson CM, Vendruscolo M. Characterization of the nucleation barriers for protein aggregation and amyloid formation. HFSP J. 2007; 1(2):137–146. [PubMed: 19404419]
20. Li MS, Klimov D, Straub J, Thirumalai D. Probing the mechanisms of fibril formation using lattice models. J Chem Phys. page accepted, 2008.
21. Sawaya MR, Sambashivan S, Nelson R, Ivanova MI, Sievers SA, Apostol MI, Thompson MJ, Balbirnie M, Wiltzius JJW, McFarlane HT, Madsen AO, Riekel C, Eisenberg D. Atomic structures of amyloid cross-beta spines reveal varied steric zippers. Nature. 2007; 447(7143):453– 457. [PubMed: 17468747]
22. Sugita Y, Kitao A, Okamoto Y. Multidimensional replica-exchange method for free-energy calculations. J Chem Phys. 2000; 113(15):6042–6051.
23. Rhee YM, Pande VS. Multiplexed-replica exchange molecular dynamics method for protein folding simulation. Biophys J. 2003; 84(2):775–786. [PubMed: 12547762]
24. Williams AD, Shivaprasad S, Wetzel R. Alanine scanning mutagenesis of a beta(1-40) amyloid fibril stability. J Mol Biol. 2006; 357(3):1283–1294. [PubMed: 16476445]
25. Nichols MR, Moss MA, Reed DK, Lin WL, Mukhopadhyay R, Hoh JH, Rosenberry TL. Growth of beta-amyloid(1-40) protofibrils by monomer elongation and lateral association. characterization of distinct products by light scattering and atomic force microscopy. Biochem. 2002; 41(19):6115–6127. [PubMed: 11994007]
26. Collins SR, Douglass A, Vale RD, Weissman JS. Mechanism of prion propagation: Amyloid growth occurs by monomer addition. PLOS Biol. 2004; 10(2):1582–1590.
27. MacKerell AD, Bashford D, Bellott M, Dunbrack RL, Evanseck JD, Field MJ, Fischer S, Gao J, Guo H, Ha S, Joseph-McCarthy D, Kuchnir L, Kuczera K, Lau FTK, Mattos C, Michnick S, Ngo T, Nguyen DT, Prodhom B, Reiher WE, Roux B, Schlenkrich M, Smith JC, Stote R, Straub J, Watanabe M, Wiorkiewicz-Kuczera J, Yin D, Karplus M. All-atom empirical potential for molecular modeling and dynamics studies of proteins. J Phys Chem B. 1998; 102(18):3586–3616. [PubMed: 24889800]
28. Mackerell AD, Feig M, Brooks CL. Extending the treatment of backbone energetics in protein force fields: Limitations of gas-phase quantum mechanics in reproducing protein conformational distributions in molecular dynamics simulations. J Comp Chem. 2004; 25(11):1400–1415. [PubMed: 15185334]
29. Im W, Lee MS, Brooks CL III. Generalized born model with a simple smoothing function. J Comput Chem. 2003; 24:1691–1702. [PubMed: 12964188]
30. Brooks BR, Bruccoleri RE, Olafson BD, States DJ, Swaminathan S, Karplus M. J Comp Chem. 1983; 4:187–217.
31. Weatherly GT, Pielak GJ. Second virial coefficients as a measure of protein-osmolyte interactions. Prot Sci. 2001; 10:12–16.
32. Auton M, Bolen DW. Additive transfer free energies of the peptide backbone unit that are independent of the model compound and the choice of concentration scale. Biochemistry. 2004; 43(5):1329–1342. [PubMed: 14756570]
33. Auton M, Holthauzen LMF, Bolen DW. Anatomy of energetic changes accompanying urea-induced protein denaturation. Proc Natl Acad Sci USA. 2007; 104(39):15317–15322. [PubMed: 17878304]

34. Frenkel, D.; Smit, B. Understanding Molecular Simulation: From Algorithms to Applications. 2. Academic Press; San Diego, Ca: 2002.
35. Frenkel D, Mooij GCAM, Smit B. Novel scheme to study structural and thermal properties of continuously deformable molecules. J Phys Cond Mat. 1992; 4(12):3053–3076.
36. Veitshans T, Klimov D, Thirumalai D. Protein folding kinetics: Timescales, pathways and energy landscapes in terms of sequence-dependent properties. Fold Des. 1997; 2(1):1–22. [PubMed: 9080195]
37. Ferrenberg AM, Swendsen RH. Phys Rev Lett. 1989; 63:1195–1198. [PubMed: 10040500]
38. Kumar S, Bouzida D, Swendsen RH, Kollman PA, Rosenberg JM. The weighted histogram analysis method for free-energy calculations on biomolecules .1. the method. J Comp Chem. 1992; 13(8):1011–1021.
39. Frishman D, Argos P. Knowledge-based protein secondary structure assignment. Proteins. 1995; 23(4):566–579. [PubMed: 8749853]
40. Yancey PH, Clark ME, Hand SC, Bowlus RD, Somero GN. Living with water-stress-evolution of osmolyte systems. Science. 1982; 217(4566):1214–1222. [PubMed: 7112124]
41. Arakawa T, Timasheff SN. The stabilization of proteins by osmolytesthe stabilization of proteins by osmolytes. Biophys J. 1985; 47(3):411–414. [PubMed: 3978211]
42. Yand DS, Yip CM, Huang THJ, Chakrabartty A, Fraser PE. Manipulating the amyloid-beta aggregation pathway with chemical chaperones. J Biol Chem. 1999; 274(46):32970– 32974. [PubMed: 10551864]
43. Hamada D, Dobson CM. A kinetic study of beta-lactoglobulin amyloid fibril formation promoted by urea. Prot Sci. 2002; 11(10):2417–2426.
44. Knowles TPJ, Shu WM, Devlin GL, Meehan S, Auer S, Dobson CM, Welland ME. Kinetics and thermodynamics of amyloid formation from direct measurements of fluctuations in fibril mass. Proc Natl Acad Sci USA. 2007; 104(24):10016–10021. [PubMed: 17540728]
45. Wolff SD, Balaban RS. Regulation of the predominant renal medullary organic solutes in vivo. Annu Rev Physiol. 1990; 52:727–746. [PubMed: 2184774]
46. Wallqvist A, Covell DG, Thirumalai D. Hydrophobic interactions in aqueous urea solutions with implications for the mechanism of protein denaturation. J Am Chem Soc. 1998; 120(2):427–428.
47. O'Brien EP, Dima RI, Brooks B, Thirumalai D. Interactions between hydrophobic and ionic solutes in aqueous guanidinium chloride and urea solutions: Lessons for protein denaturation mechanism. J Am Chem Soc. 2007; 129(24):7346–7353. [PubMed: 17503819]

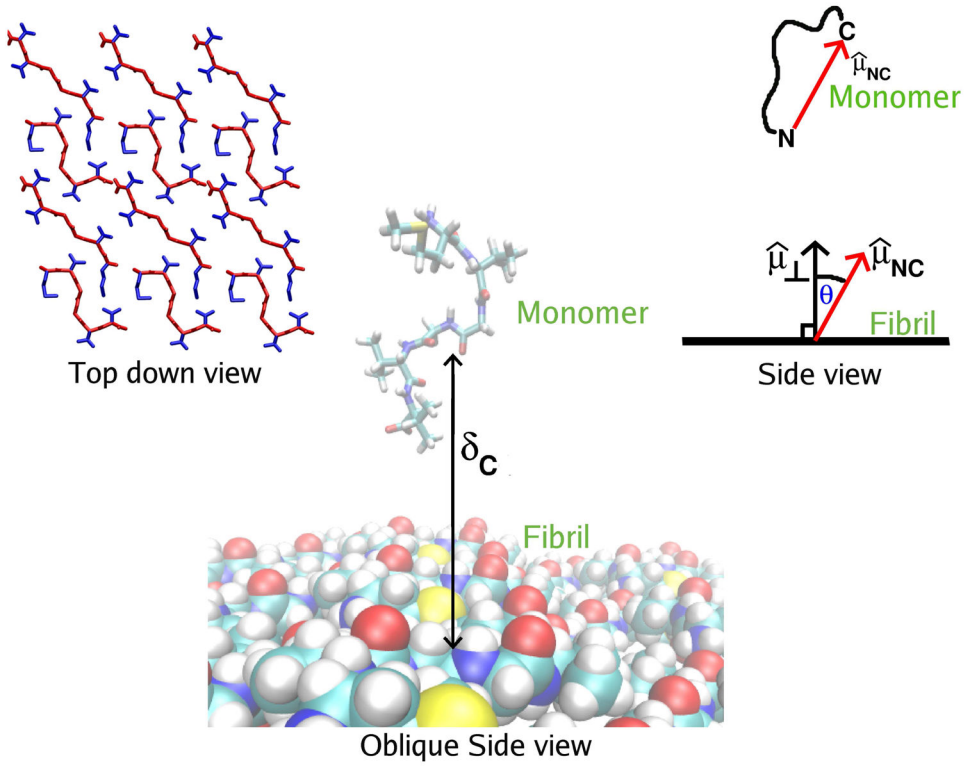

Figure 1.

Monomer addition to an amyloid fibril. 'Top down view' shows the peptides in the fibril surface from above. The peptides are displayed as sticks with backbone atoms in red and side chain atoms in blue. 'Oblique side view' shows the fibril surface in a van der Walls representation while the unincorporated monomer is shown in a stick representation. 'Side view' offers a simple geometric perspective of the fibril surface and monomer from the side to illustrate the calculation of the θ-angle (see Methods). The vector normal to the fibril surface is shown as a black arrow, while the monomers N-to-C termini vector is shown as a red arrow. θ is the angle formed by these two vectors. The $cos(\theta)$ term used in Fig. 4B is equal to $\hat{\mu_{NC}} \cdot \hat{\mu_{\perp}} / (|\hat{\mu_{NC}}||\hat{\mu_{\perp}}|)$.

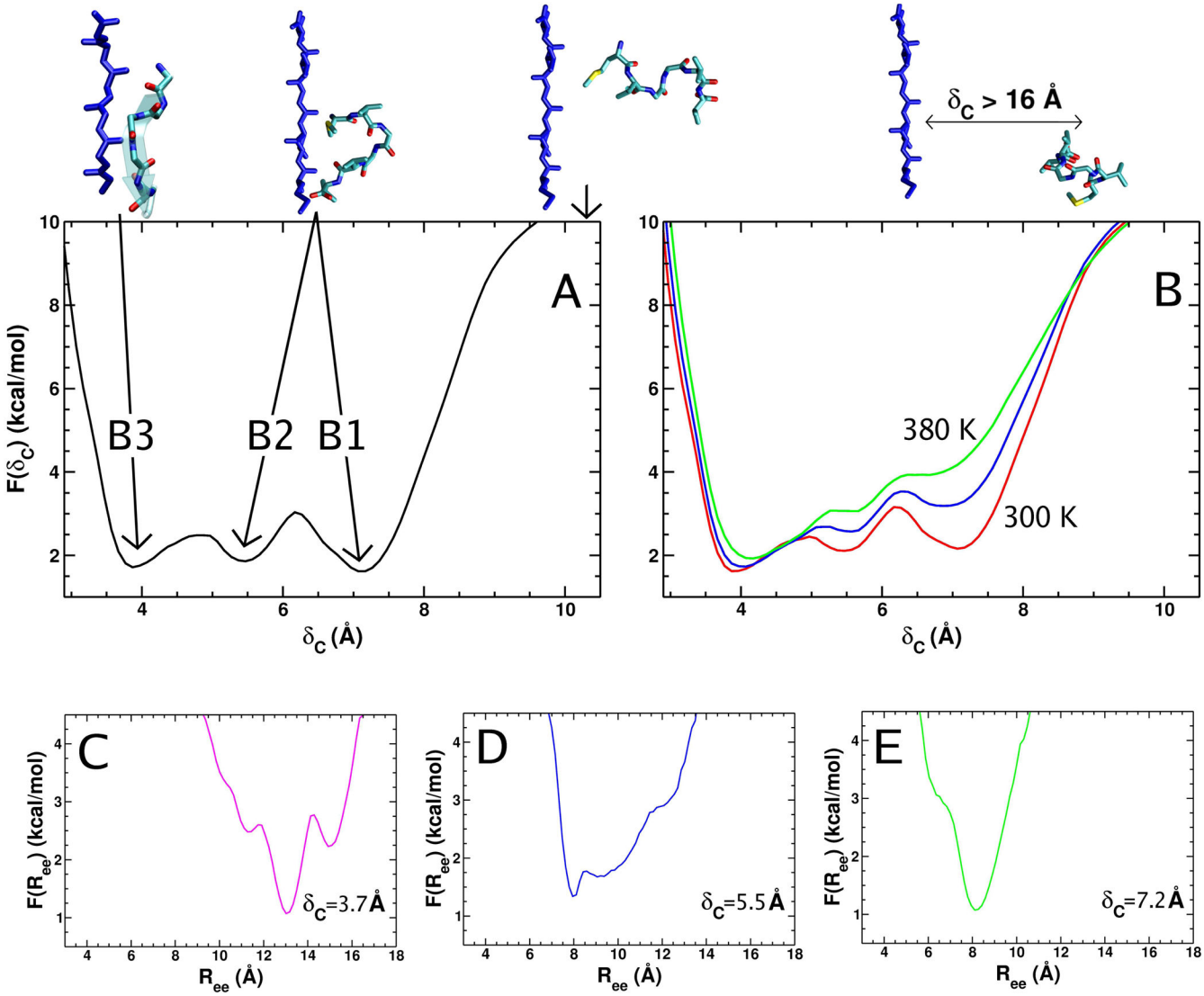

Figure 2.

The free energy profile ($F(\delta_C) = -k_BT\, ln[Z(\delta_C)/Z]$) of monomer addition as a function of δ_C. (A) The temperature is 280 K. (B) The curves correspond are at temperatures of 300 K (red line), 340 K (blue line), and 380 K (green lines). Representative structures in the free energy basins B1, B2 and B3 labelled in (A) are shown. In addition, two monomer-fibril configurations that have δ_C > 10 Å are also shown. A peptide in the fibril surface is shown in blue, while the docking monomer is displayed in non-blue colors. Note that the underlying fibril (blue) peptide is of the extended form (see the 'Top down view' in Fig. 1) for all structures except the one corresponding to the B1 basin. In this structure the underlying fibril peptide is of the reverse 'S' shape form (Fig. 1). The free energy profile as a function of the monomer end-to-end distance at a specified δ_C ($F(R_{ee}|\delta_C) = -k_BT\, ln[Z(R_{ee}|\delta_C)/Z(\delta_C)]$) is shown for δ_C = 3.7, 5.5, and 7.2 Å (i.e. for basins B1, B2 and B3 in (A)) in (C), (D), and (E) respectively.

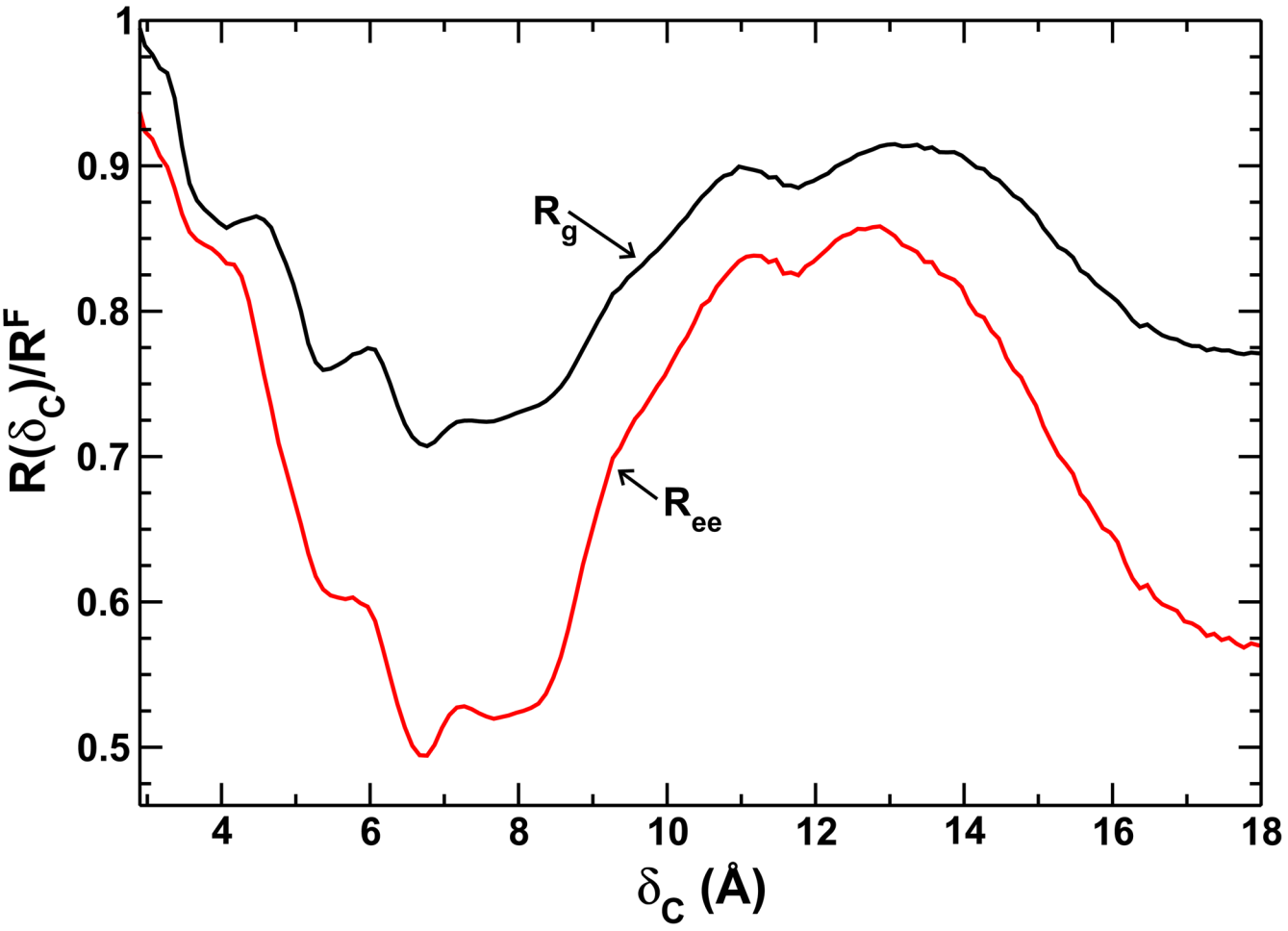

Figure 3.

The radius-of-gyration (R_g) of the monomer, scaled by its average value of 7.2 Å in the fibril surface (R_g^F), as a function of δ_C in bulk is shown in black. The red curve shows R_{ee} of the monomer, scaled by its average value of 15.4 Å in the fibril surface (R_{ee}^F), as a function of δ_C. The temperature is 300 K.

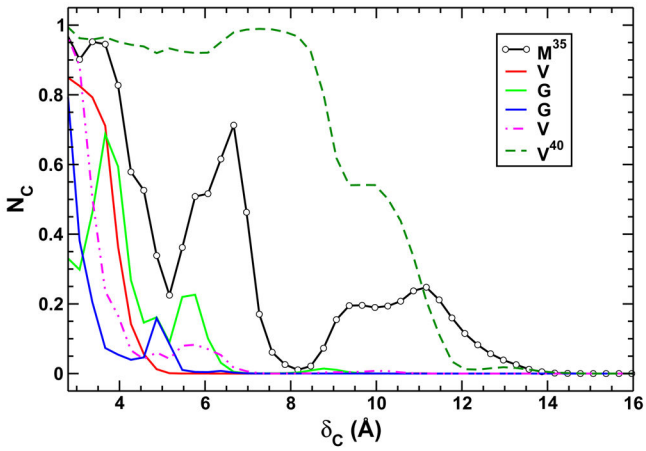

(a)

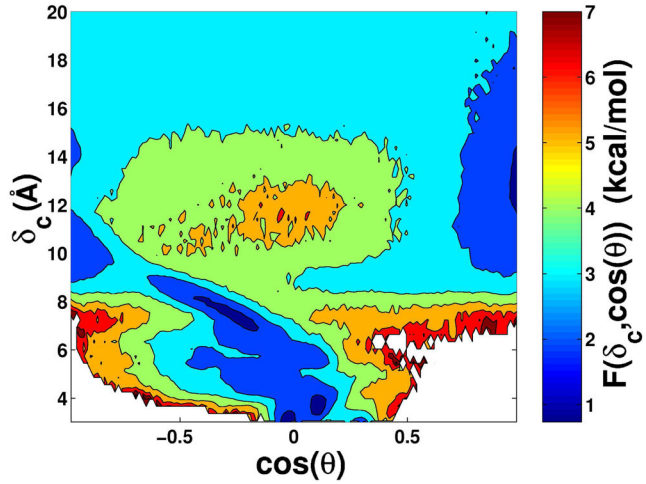

(b)

Figure 4.

(A) The number of anti-parallel in-register backbone-backbone contacts between the monomer and fibril as a function of δ_C. The symbols for the various residues starting from the *N*-terminal methionine are shown in the legend. (B) The free energy surface ($F(\delta_C, cos(\theta)) = -k_BT\, ln[Z(\delta_C,\theta)/Z(\delta_C)]$) as a function of δ_C and $cos(\theta)$ at 340 K. θ is the angle formed by a vector normal to the plane of the fibril surface and the *N* to *C* terminal vector of the monomer (see Fig. 1).

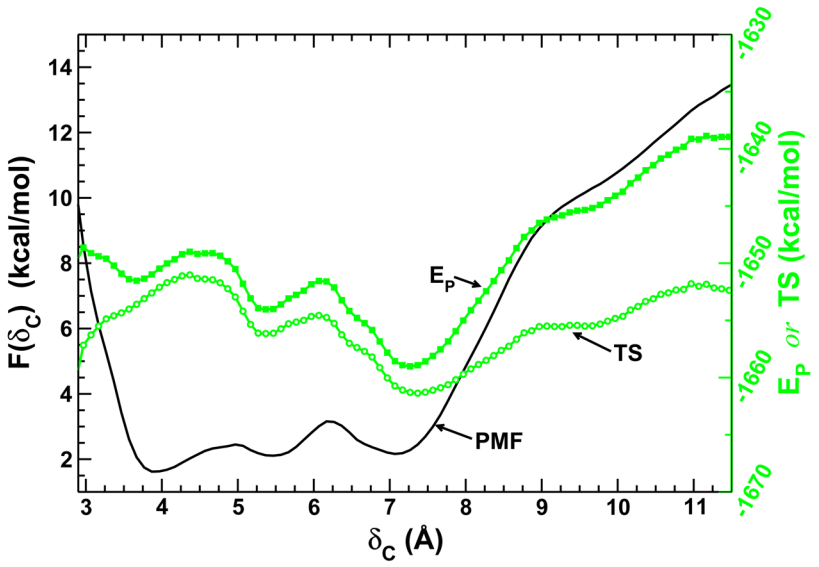

(a)

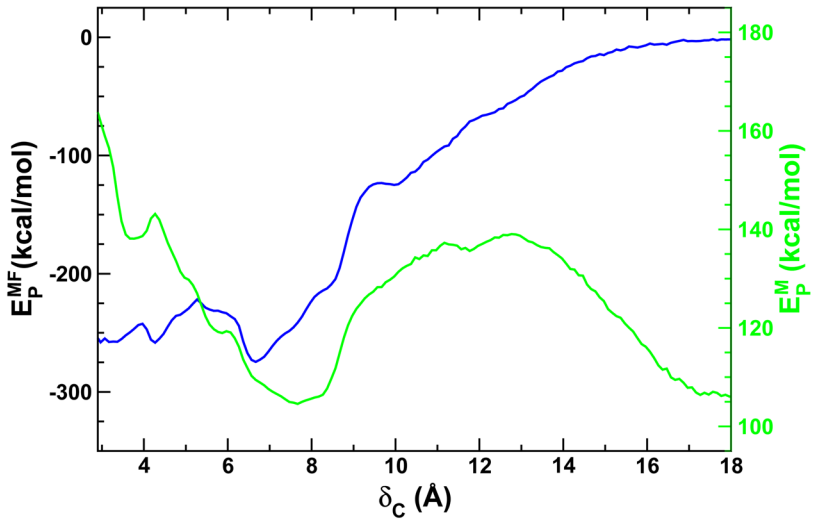

(b)

Figure 5.

(A) Deconvolution of F (δ_C) into entropic ($TS(\delta_C)$) and energetic (E_P (δ_C)) components as a function of δ_C at 300 K. The δ_C-profile of each term is indicated on the graph. (B) The interaction energy between the monomer and the fibril (E_P^{MF}, blue lines), and monomer's intrapeptide interaction (E_P^M) as a function of δ_C at 300 K. Bulk (ϕ_C =0.00) and crowded (ϕ_C =0.14) conditions are shown as solid and dashed lines respectively.

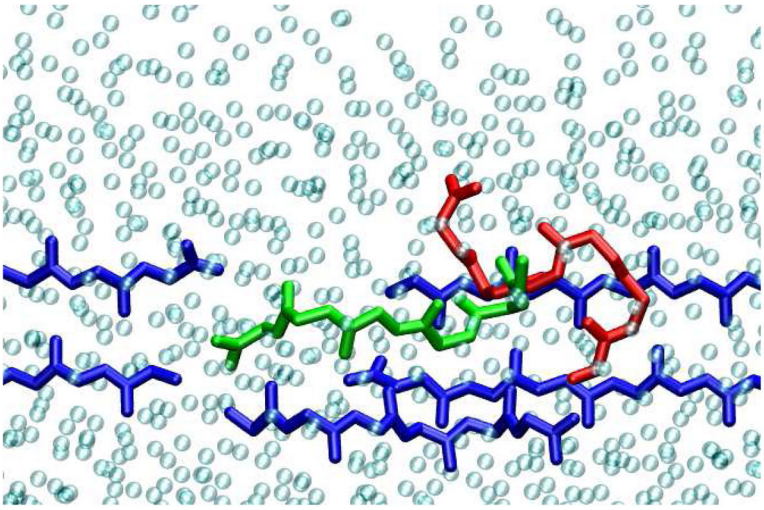

Figure 6.

Illustration of the finite width fibril used in the explicit solvent simulations. The fibril is three β-sheets wide, with the restrained peptides shown in blue and the unrestrained monomer shown in green and red. The green and red peptides are the final structures after 45 ns of simulation time from trajectories that were initiated from the crystal and displaced configurations respectively (see Methods section for details). Note that the trajectory started from the crystal structure (green monomer) loses ordered hydrogen bonds with the fibril at one end. Water molecules are shown as transparent cyan spheres centered on the water oxygens.

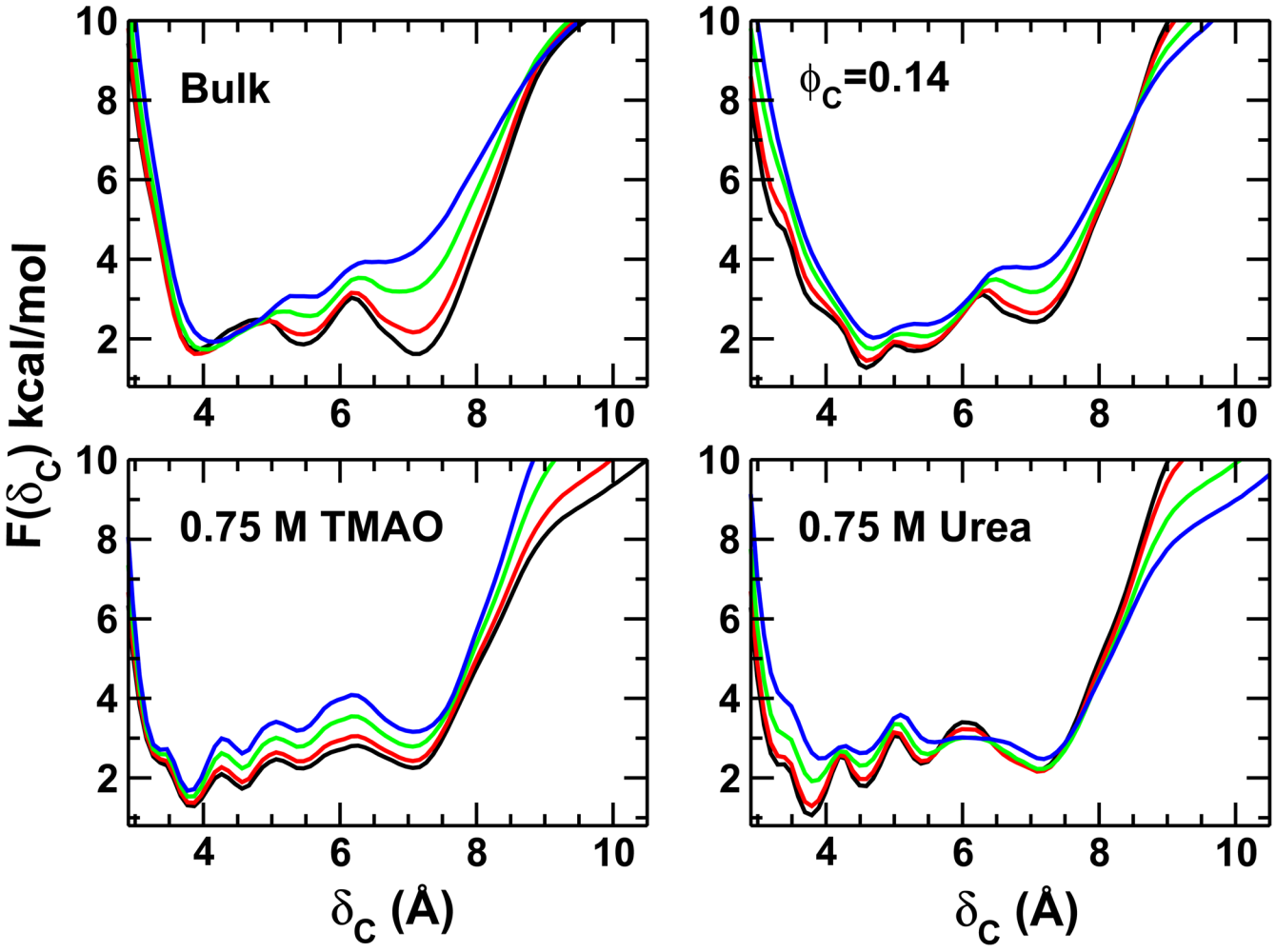

Figure 7.

The free energy profile F (δ_C) at temperatures of 280 K (black line), 300 K (red line), 340 K (green line), and 400 K (blue line) for (A) Bulk solution, (B) crowded solution, (C) aqueous TMAO and (D) urea solutions. The relative values of the critical monomer concentration are calculated from these profiles using Eq. 8.

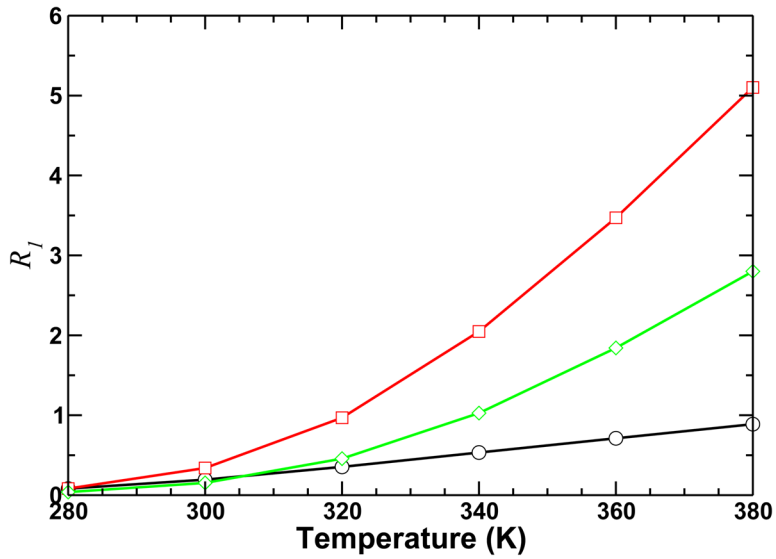

(a)

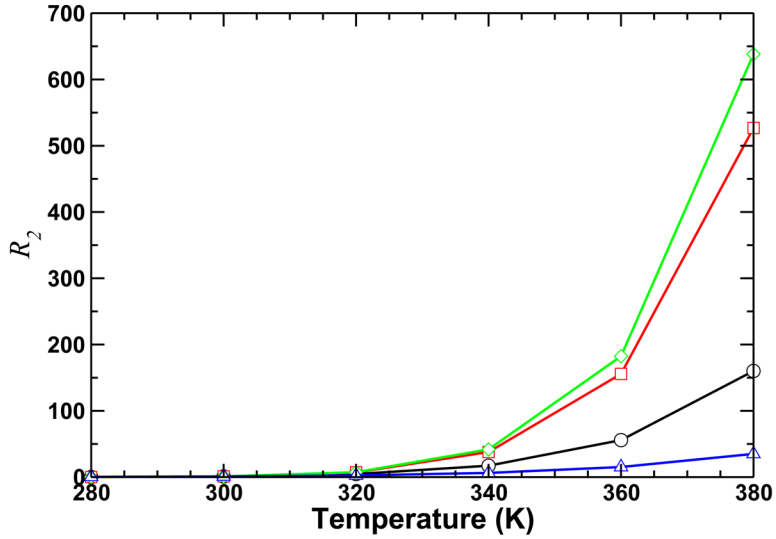

(b)

Figure 8.

The ratio of critical concentrations $R_1(= C_R(T\,|Cosolute)/C_R(T\,|Bulk))$ and $R_2(= C_R(T)/C_R(T = 300\,K))$ are shown in (A) and (B) respectively. Solution conditions are ϕ_C = 0.14, 0.75 M urea, 0.75 M TMAO, and bulk are shown as, respectively, black circles, red squares, green diamonds, and blue triangles. Lines are to guide the eye.

TABLE I

Lennard-Jones parameters for urea and TMAO particle interactions with peptide atoms used in $4\varepsilon_{ij}[(\sigma_{ij}/r_{ij})^{12} - (\sigma_{ij}/r_{ij})^{6}]$.

Atom Type i[a]	$\varepsilon_{i,urea}$[b]	$\varepsilon_{i,TMAO}$
CT1	0.0924875	0.074005
CT2	0.0924875	0.074005
CT3	0.091795	0.085255
CT4[c]	0.0859	0.08521
CT5	0.0924875	0.074005
C	0.09162	0.059
O	0.09162	0.059
NH1	0.09162	0.059
H	0.022905	0.01475
HB	0.022905	0.01475
S	0.098	0.10725
HA	0.02294875	0.02131375

[a] Atom names, unless otherwise indicated, are the same as in the CHARMM 22 force-field [27]. Lorentz-Brethlot mixing rules are used for all other atoms [30].

[b] $\varepsilon_{i,urea}$ and $\varepsilon_{i,TMAO}$ are in units of *kcal/mol*.

[c] Atoms CT4 and CT5 are new atom types added to the CHARMM 22 force-field. CT4 and CT5 have the exact same properties as atoms CT2 and CT3, respectively, except for the Lennard-Jones parameters listed in this table. CT4 replaces CT2 in the valine residue. CT5 replaces CT3 in the methionine side chain.